Available online at www.sciencedirect.com
SCIENCE DIRECT®
ELSEVIER
International Journal of Solids and Structures 42 (2005) 5259–5273
INTERNATIONAL JOURNAL OF SOLIDS and STRUCTURES
www.elsevier.com/locate/ijsolstr

The electro-mechanical response of highly compliant substrates and thin stiff films with periodic cracks

Matthew R. Begley [a,*], Hilary Bart-Smith [b]

[a] Structural and Solid Mechanics Program, Department of Civil Engineering, University of Virginia, Charlottesville, VA 22904, USA
[b] Department of Mechanical and Aerospace Engineering, University of Virginia, Charlottesville, VA 22904, USA

Received 23 April 2004; received in revised form 10 February 2005
Available online 28 April 2005

Abstract

We present results that describe the mechanical response of highly compliant substrates coated with ultra-thin stiff films, with thickness and elastic moduli differences spanning four orders of magnitude. Dimensional analysis based on shear-lag models of cracked films is used to identify key parameters that control the effective elastic properties of the cracked multi-layer, crack opening displacements, and the steady-state energy release rate for channeling crack formation. Analytical forms that describe multi-layer response in terms of film properties and crack spacing are presented and corroborated with numerical models for linear elastic materials. A key result is that the energy release rate scales with $1/(1-\alpha)$, where α is one of the Dundurs' parameters describing elastic mismatch. The results can also be used to evaluate the performance of electrostrictive actuators comprised of cracked blanket electrodes and elastomer dielectrics. In this scenario, an interesting result is that ultra-thin cracked films can continue to distribute charge, since crack openings may be small enough to allow breakdown in air at typical operating voltages.

Keywords: Elastomers; Channel cracking; Effective moduli; Multi-layers

1. Introduction

Highly compliant multi-layers are increasingly prevalent, particularly in electrostrictive polymer actuators designed to exploit the compliance and near incompressibility of the substrate to achieve large strains (e.g. Pelrine et al., 1998, 2000). Fig. 1a shows a schematic illustration of such a device, which is comprised of

* Corresponding author. Tel.: +1 434 243 8728; fax: +1 434 982 2951.
E-mail address: begley@virginia.edu (M.R. Begley).

0020-7683/$ - see front matter © 2005 Published by Elsevier Ltd.
doi:10.1016/j.ijsolstr.2005.02.014

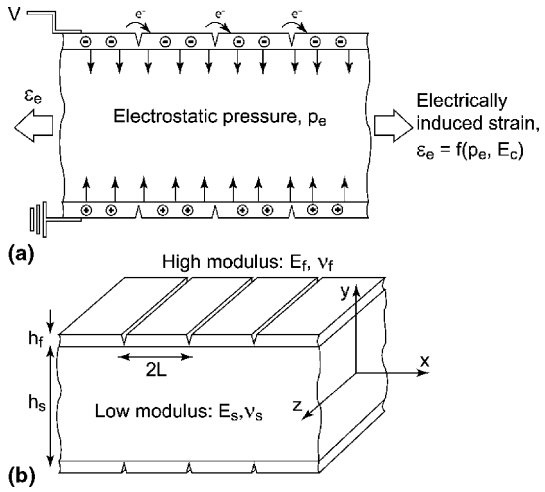

Fig. 1. (a) Schematic illustration of an electrostrictive actuator comprised of a highly compliant material (dielectric) sandwiched between conductive layers (electrodes). (b) Illustration of the cracked multilayer geometry under consideration.

a compliant thick layer sandwiched between stiff, thin conductive layers. An electric field applied across the layers causes attraction between the electrodes and generates an electrostatic pressure that squeezes the middle layer and lengthens the film.

The in-plane strain that is developed is a function of the strength of the electric field, the dimensions of the electrodes and dielectric, and critically the effective in-plane modulus of the multi-layer. The function of the conductive layers is purely to hold charge; ideally, the electrodes should be as compliant as possible so as to not limit the actuation strain. This implies that ultra-thin films with low stiffness are desirable for use as the electrode. Micro-patterning of the conductive layers is one effective approach to reduce the stiffness of conductive metal layers (Pelrine et al., 1998).

Alternatively, cracking of a blanket layer (which is far easier to fabricate) can reduce the effective in-plane modulus of the multi-layer. In this case, one must consider charge distribution across the cracked electrode. The key factor is the size of the crack opening. For sufficiently small crack openings, dielectric breakdown of the air in the cracks occurs and conduction functionality is maintained, as shown schematically in Fig. 1a. It should be emphasized that this occurs only at relatively small in-plane strains (less than about 10%); for sufficiently large in-plane strains, the cracked layer will not be capable of distributing charge. As such, the cracked electrode concept is applicable to scenarios where relatively small actuation strains are useful, such as controlling the transverse stiffness of a freestanding membrane. This is discussed in detail in Section 5.

In addition to scenarios where cracking can enhance performance, the mechanical response of cracking in thin brittle films bonded to highly compliant substrates is relevant to film toughness measurements. The film toughness can be determined by the measuring the saturation crack spacing and relating it to the energy release rate for a periodic array of cracks (e.g. Thouless, 1990; Delannay and Warren, 1991; Hutchinson and Suo, 1992; Nahta and Moran, 1995). For very tough (or very thin films), residual stresses created during deposition on stiff substrates (e.g. silicon or metal) may not be large enough to crack the film. Moreover, brittle substrates may crack before mechanical loading of the multi-layer generates sufficient film stress. In contrast, large stresses can be induced in films on highly compliant layers via mechanical loading, without substrate failure.

In this paper, we model the mechanical response of cracked multi-layers with highly compliant substrates, as shown in Fig. 1b. For simplicity and the sake of comparison with previous results on film crack-

ing, we consider the plane-strain response of the cracked multi-layer with $\varepsilon_z = 0$. Three key results are presented:

(i) A description of the stress–strain response of the multi-layer in terms of elastic properties, crack spacing and film thickness; this will provide critical input to models of electro-mechanical actuator performance.
(ii) Relationships between crack openings, applied stress, elastic properties, crack spacing and film thickness; these can be used to estimate critical loading parameters that determine when electrical functionality is lost.
(iii) Relationships between applied stress, elastic properties, crack spacing and film thickness, and the steady-state energy release rate governing the formation of channel cracks.

As one would expect, there is a vast amount of previous work on the mechanics of cracked multi-layers, both with regards to the formation of channeling cracks (e.g. Thouless, 1990; Delannay and Warren, 1991; Hutchinson and Suo, 1992; Nahta and Moran, 1995) and the overall constitutive response (e.g. McCartney et al., 2000). The principle difference between previous analyses and those presented here is on the severity of the elastic mismatch between the substrate and film. This mismatch has a profound effect on crack opening displacements; as will be illustrated, previous results cannot be extrapolated to the present regime without the analyses considered here.

It has been well established for linear elastic materials that the two dimensionless Dundurs' parameters for the film/substrate multi-layer fully describe the role of elastic properties:

$$\alpha = \frac{\overline{E}_f - \overline{E}_s}{\overline{E}_f + \overline{E}_s}, \tag{1a}$$

where $\overline{E}_s = E_s/(1 - v_s^2)$ and $\overline{E}_f = E_f/(1 - v_s^2)$ are the plane-strain moduli of the substrate and film, respectively, and

$$\beta = \frac{E_f(1 + v_s)(1 - 2v_s) - E_s(1 + v_f)(1 - 2v_f)}{E_f(1 + v_s)(1 - v_s) + E_s(1 + v_f)(1 - v_f)}. \tag{1b}$$

For metals or polymer films on elastomer substrates, the modulus mismatch is on the order of $\overline{E}_f \sim (10^2\text{–}10^5)\overline{E}_s$, which in turn implies $\alpha = 1 - \eta$, where $\eta \sim 10^{-2}\text{–}10^{-5}$. Previous works have considered mismatch only as large as $\alpha = 0.99$ (Beuth, 1992; Huang et al., 2003). As will be shown, the steady-state energy release rate for the formation of channeling cracks scales with $1/(1 - \alpha)$, indicating that new solutions are needed for larger α values, despite seemingly negligible differences when $\alpha \approx 1$. For such material combinations and when the substrate is nearly incompressible (i.e. $v_s \to 1/2$), β is typically $<\sim 0.02$.

The limit where $\alpha \to 1$ has important implications with regards to the role of multi-layer geometry. As will be demonstrated, an important dimensionless parameter that influences the mechanical response of the multi-layer is

$$S = \frac{h_f \overline{E}_f}{h_s \overline{E}_s}. \tag{2}$$

This parameter indicates the relative stiffness contributions of the two layers to the overall stiffness of the multi-layer. Most previous studies of film cracking have considered scenarios with semi-infinite substrates, implying that $S \to 0$ (e.g. Thouless, 1990; Delannay and Warren, 1991; Beuth, 1992; Hutchinson and Suo, 1992). Those that have considered finite thickness substrates have not considered the mechanical response of the cracked multi-layer (e.g. Nahta and Moran, 1995) and/or the extremely large mismatch considered here (e.g. Nahta and Moran, 1995; McCartney et al., 2000). The fact that the modulus ratio is so large implies that seemingly negligible film thickness (or conversely, seemingly semi-infinite substrates) can still

have a significant impact on the overall mechanical response. For example, a 1 nm thick gold film on top of an elastomer 10^5 nm thick yields $S \approx 10$, indicating the 1 nm thick film dominates the mechanical response.

Another important consideration when elastic mismatch is severe concerns the interaction between individual cracks in a periodic array. A more moderate mismatch implies that individual cracks in a periodic array have a negligible influence on their neighbors when the crack spacing exceeds the film thickness by about two orders of magnitude. In the present scenario, crack interaction is strongly influenced by the crack spacing relative to the substrate thickness. Crack interaction is important for crack spacing that is several orders of magnitude larger than the film thickness.

Despite the fact that the motivation is principally metal and polymer films on elastomers, we model both materials as linear elastic. It is likely that including non-linear elastic behavior—more appropriate for elastomers—will modify the present results, even at small-applied stress, because of the large strains experienced at the crack tip(s). However, the principal motivation here is to determine critical non-dimensional parameters that capture the role of film thickness and elastic mismatch.

2. Key dimensionless parameters and functional forms

This section presents a shear-lag model (e.g. Hutchinson and Jensen, 1990; Beuth and Klingbeil, 1996) for the film that yields dimensionless parameters that control the effective modulus of the cracked multi-layer, crack opening, and energy release rates. The analysis yields simple functional forms that can be used to describe the mechanical response in terms of the layer thickness, elastic properties and crack spacing. The model is based on the assumption that the film thickness is much smaller than the substrate, such that shear transfer between the matrix and film is confined to a small region along the interface and near the crack. Fig. 2 provides a schematic illustration of the model, which includes two regions: (i) a shear transfer region where the film stresses increase from zero at the crack,[1] and (ii) a region of intact response where strain is uniform.

The analysis is valid for a two layer system confined from bending, or the symmetric three layer system shown in Fig. 1b, subjected to a uniform displacement condition in the x-direction at the outer boundaries. This model can be thought of as either a single crack in a substrate of width L, or a periodic array of cracks with spacing $2L$. A simple one-dimensional shear-lag analysis yields the stress, strain and displacement distributions in the x-direction.

2.1. Mechanical response of multi-layers with cracked films

The analysis assumes that the deformation in the multi-layer is uniform in the y-direction and zero in the z-direction, such that only the x-direction must be considered. Equilibrium in the x-direction implies

$$\hat{h}_f \sigma_f(x) + \hat{h}_s \sigma_s(x) = \sigma, \tag{3}$$

where $\hat{h}_f = h_f/(h_f + h_s)$, $\hat{h}_s = h_s/(h_f + h_s)$ and P is the force per unit width applied to the multi-layer, such that $\sigma = P/(h_f + h_s)$ is the average stress acting on the multi-layer. If the multi-layer is intact, the stress–strain relationship is given by

$$\sigma = \left[\hat{h}_f \overline{E}_f + \hat{h}_s \overline{E}_s\right] \varepsilon = \overline{E}_0 \varepsilon, \tag{4}$$

where $\overline{E}_0$ is the effective plane strain modulus of the intact multi-layer, and ε is the macroscopic strain.

[1] This region corresponds to the portion of the interface that has slipped in frictional sliding analyses (e.g. Hutchinson and Jensen, 1990), or yielding when the substrate is elastic–plastic (e.g. Beuth and Klingbeil, 1996).

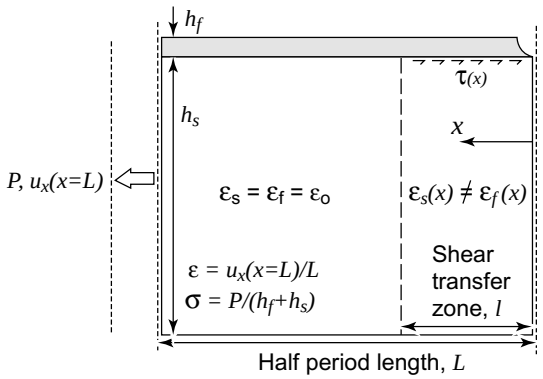

Fig. 2. Schematic diagram of the shear-lag model used to identify key dimensionless parameters; the model has fixed displacements in the vertical direction along the bottom edge, and symmetry implies the results are valid for the three-layer system shown in Fig. 1.

A shear-lag analysis assumes that the direct stress is uniform through the thickness, and the shear stress varies linearly from that at the interface to zero at the top surface of the film. In the *shear transfer region*, equilibrium implies that the direct stress in the film is equal to the integral of the shear stress along the interface. Here, we assume that the shear traction along the bimaterial interface is an unknown function *that scales with the average remote stress*, σ. The exact form of this function is not known, and as will be demonstrated, it is not important to the present analysis. The stress in the film can then be written as

$$\sigma_{\mathrm{f}}(x) = \int_0^x \frac{\tau(\tilde{x})}{h_{\mathrm{f}}}\mathrm{d}\tilde{x} = \frac{\sigma}{h_{\mathrm{f}}}\int_0^x f(\tilde{x})\mathrm{d}\tilde{x} = \frac{\sigma \cdot l}{h_{\mathrm{f}}}\phi'(\bar{x}), \tag{5}$$

where $\bar{x} = x/l$ and $f(x)$ and $\phi'(\bar{x})$ are dimensionless functions. l is the shear transfer length, defined as the distance from the crack tip at which the strain in the film and substrate are equal. Eq. (3) can be used to write a similar result for the stress in the substrate:

$$\sigma_{\mathrm{s}}(\bar{x}) = \frac{\sigma}{\hat{h}_{\mathrm{s}}} - \frac{\hat{h}_{\mathrm{f}}}{\hat{h}_{\mathrm{s}}}\frac{\sigma \cdot l}{h_{\mathrm{f}}}\phi'(\bar{x}). \tag{6}$$

The shear transfer length is determined by the requirement that the strains in the film and matrix are equal at $x = l$, and governed by the average stress at the outer boundary. This implies

$$\varepsilon_{\mathrm{s}}(\bar{x}=1) = \varepsilon_{\mathrm{f}}(\bar{x}=1) = \frac{\sigma}{\overline{E}_0}. \tag{7}$$

After dividing Eqs. (5) and (6) by the appropriate moduli and simplifying, one obtains

$$l = \frac{1}{\phi'(1)}\frac{h_{\mathrm{f}}\overline{E}_{\mathrm{f}}}{\overline{E}_0}, \tag{8}$$

where $\phi'(1)$ is a dimensionless constant. The strain of the cracked section (of width L) is then defined in terms of the total displacement of the left boundary (see Fig. 2):

$$\varepsilon = \frac{u_x(x=L)}{L} = \frac{1}{L}\left[(L-l)\frac{\sigma}{\overline{E}_0} + u_{\mathrm{s}}(x=l)\right], \tag{9}$$

where $u_{\mathrm{s}}(x=l)$ is the displacement of the substrate at the edge of the shear transfer region. Dividing Eq. (6) by the substrate modulus and integrating yields the following:

$$u_s(\bar{x}) = \frac{\sigma \cdot l}{\overline{E}_s \hat{h}_s}\bar{x} - \frac{\hat{h}_f}{\hat{h}_s}\frac{\sigma \cdot l^2}{\overline{E}_s h_f}\int_0^{\bar{x}} \phi'(\tilde{x})\,d\tilde{x} = \frac{\sigma \cdot l}{\overline{E}_s \hat{h}_s}\bar{x} - \frac{\hat{h}_f}{\hat{h}_s}\frac{\sigma \cdot l^2}{\overline{E}_s h_f}\phi(\bar{x}), \tag{10}$$

where once again the shear transfer length has been used to normalize the integral, such that $\phi(\bar{x})$ is dimensionless. Combining Eqs. (8)–(10) and performing algebraic gymnastics produces the final result:

$$\varepsilon = \frac{\sigma}{\overline{E}_0}\left[1 + c\left(\frac{h_f \overline{E}_f}{L\overline{E}_s}\right)\left(\frac{\hat{h}_f \overline{E}_f}{\hat{h}_s \overline{E}_0}\right)\right], \tag{11}$$

where the constant c is given by

$$c = \frac{1}{\phi'(1)}\left(1 - \frac{\phi(1)}{\phi'(1)}\right). \tag{12}$$

An alternative way of interpreting Eq. (11) is to consider the effective modulus of the cracked multi-layer, defined via $\sigma = \overline{E}_c \varepsilon$; this is given by

$$\frac{\overline{E}_c}{\overline{E}_0} = \left[1 + c\left(\frac{h_f \overline{E}_f}{L\overline{E}_s}\right)\left(\frac{\hat{h}_f \overline{E}_f}{\hat{h}_s \overline{E}_0}\right)\right]^{-1}. \tag{13}$$

For thin films where $h_f \ll h_s$ and compliant substrates where $\overline{E}_s \ll \overline{E}_f$, $\hat{h}_f \overline{E}_f \cong \hat{h}_s \overline{E}_0$, such that the second dimensionless quantity is approximately unity. Eq. (13) represents a key result, as it completely captures the influence of thickness, elastic properties and crack spacing on the effective modulus of the cracked multi-layer.

For high crack densities (small crack spacing), the shear transfer zones from adjacent cracks overlap, and the shear transfer length, l, is equal to the crack spacing, L. Setting them equal to one another and repeating the analysis, Eq. (6) yields following:

$$\frac{\overline{E}_c}{\overline{E}_s \hat{h}_s} = \left[1 - \phi_1'(1)\left(\frac{L}{h_s}\right)\right]^{-1} = 1 + \phi_1'(1)\left(\frac{L}{h_s}\right) + O\left[\left(\frac{L}{h_s}\right)^2\right]. \tag{14}$$

Note that here the effective modulus of the cracked multi-layer is normalized in terms of the effective modulus of just the substrate. It should be emphasized that this analysis is based on the assumption that the interface shear stress scales with the average stress (σ) at $x = L$. This is merely an approximation, since the strain in the film and substrate at this location are not necessarily equal, as they are when the edge of the shear-lag zone terminates at $x < L$. This is discussed further in Section 4.1.

2.2. Crack openings and channeling crack formation

The steady-state energy release rate controlling the formation of the channeling cracks is given by (e.g. Beuth, 1992)

$$G_{ss} = \frac{1}{h_f}\int_0^{h_f} \sigma_f^i \delta(y)\,dy, \tag{15}$$

where σ_f^i is the stress in the intact film prior to cracking (ahead of the crack), and $\delta(y)$ is the total crack opening displacement of the crack (in the wake of the crack).

The shear-lag model for the previous section can again be used to determine the dimensionless parameters controlling the energy release rate. We assume that the crack opening is approximately constant through the thickness of the film, as is typical in shear-lag analyses. The crack face displacement is equal to substrate displacement at the edge of the shear transfer zone minus the displacement of the crack face (measured relative to edge of the shear transfer zone):

$$\delta = 2(u_s(l) - u_f(l)). \tag{16}$$

The displacement in the film can be calculated from Eq. (5) (by converting to strain and integrating), while that of the substrate is found via Eq. (10). Using these results, the crack opening displacement becomes

$$\delta = ch_f\left(\frac{\overline{E}_f}{\overline{E}_s}\right)\left(\frac{\overline{E}_c}{\overline{E}_0}\right)\varepsilon, \tag{17}$$

where c is again given by Eq. (12), ε is the total strain in the multi-layer ($\varepsilon = u_x(x = L)/L$). The crack opening can be conveniently expressed in terms the crack spacing using Eq. (11).

The stress in the intact film (prior to cracking) can be expressed as $\sigma_f^i = \overline{E}_f\varepsilon$. Using Eqs. (15)–(18), the energy release rate is given by

$$G_0 = c\left(\frac{\overline{E}_f}{\overline{E}_s}\right)\left(\frac{\overline{E}_c}{\overline{E}_0}\right)\overline{E}_f\varepsilon^2 h_f = \frac{c\left(\frac{\overline{E}_f}{\overline{E}_s}\right)\overline{E}_f\varepsilon^2 h_f}{\left[1 + c\left(\frac{h_f\overline{E}_f}{L\overline{E}_s}\right)\left(\frac{h_f\overline{E}_f}{h_s\overline{E}_0}\right)\right]}. \tag{18}$$

Note that this result corresponds to result for simultaneous cracking of an array of cracks. For sequential cracking scenarios (i.e. the driving force for an array of cracks growing between previously existing cracks, as encountered in crack saturation experiments), the analysis must be modified according to the procedure outlined by Begley et al. (2005).

For comparisons with previous studies, it is interesting to note that for large elastic mismatch, $\overline{E}_f/\overline{E}_s = (1-\alpha)/2 + O[(1-\alpha)^2]$, such that for $\alpha \approx 1$:

$$G_0 = \left(\frac{2c}{1-\alpha}\right)\frac{\overline{E}_c\overline{E}_f\varepsilon^2 h_f}{\overline{E}_0}. \tag{19}$$

Thus, small deviations from $\alpha \approx 1$ lead to dramatic differences in energy release rates. In the limit of a rigid film on top of an elastic substrate, the energy release rate becomes unbounded.

Although not directly illustrated in this paper, it is interesting to note that the asymptotic crack tip fields dominate behavior near the crack tip in a highly localized region that is much smaller than the film thickness. This is most easily shown by considering the asymptotic crack opening displacements. Asymptotic analysis reveals that the crack opening displacements near the tip scale as (for $\beta = 0$) (Zak and Williams, 1963; Cook and Erdogan, 1972):

$$\delta(r) \propto \frac{\sigma \cdot h_f}{\overline{E}_f\sqrt{1-\alpha}}\left(\frac{r}{h_f}\right)^{0.88\sqrt{1-\alpha}}. \tag{20}$$

If the crack tip fields dominated over a length scale comparable to the film thickness, then one would expect $G_0 \propto 1/\sqrt{1-\alpha}$. As will be illustrated, this is clearly not the case, indicating that non-singular terms arising in asymptotic stress analysis play an important role in channeling crack formation.

3. Computational models

Finite element models of the crack layers were constructed using the commercial code ABAQUS. The symmetry plane of the crack is constrained in the x-direction and free to displace in the y-direction. A uniform x-displacement, u_x is enforced on the outer boundary, such that $\varepsilon = u_x(x = L)/L$; this appropriately enforces periodicity for an array of cracks. The left vertical boundary is free to displace in the y-direction. The bottom of model is constrained in the y-direction and free to move in the x-direction.

The meshing strategy is outlined in (Begley and Begley, 2003), which provides examples of the resulting mesh pattern. A focused radial fan mesh is included at the crack tip with a graded element distribution

towards the outer boundaries. Eight-noded plane strain quadrilaterals with reduced integration were used. The mesh consisted of 40 elements around the circumference of the crack tip, with 25 elements along an arc in the fan region. The number of elements between the focused region and the outer boundary was 50. Convergence studies have indicated this is more than sufficient to capture behavior near the crack tip singularity and accurately compute energy release rates (Begley and Begley, 2003).

The average stress at the outer boundary, σ, is computed by dividing the sum of the reaction forces generated at the outer boundary by the height of the model. The effective modulus of the cracked multi-layer was computed as $\overline{E}_c = \sigma/\varepsilon = PL/(u_x(x = L)(h_f + h_s))$. The energy release rate can be calculated via Eq. (15), by determining the stress in the film from an analysis of the intact multi-layer, and the crack opening displacements from an analysis of a traction-free cracked section. This can be done by summing the product of nodal reaction and nodal displacements (along the crack), from the intact and cracked analyses, respectively. Alternatively, one can compute the steady-state energy release rate as $G = \Delta(\text{S.E.})/h_f$, where Δ(S.E.) is the change in total strain energy (throughout the *entire* model) from the intact to the cracked analyses. This option is particularly convenient when using ABAQUS, which reports the total strain energy of the model as an output.

4. Results

Examples of the layer properties for the cases reported are shown in Table 1. The substrate properties and the first three cases are motivated by the multi-layers fabricated for electro-mechanical experiments (Begley et al., 2005).

4.1. Effective modulus of the cracked multi-layer

Fig. 3 shows the effective modulus of the cracked multi-layer relative to the effective modulus of the intact multi-layer, as a function of the normalized crack spacing. Eq. (11) is superimposed on the numerical results, with the constant $c \approx 0.2$ determined via a least squares fit. For low to moderate crack densities, the theoretical result for the effective modulus (with a single fitting parameter) is within 5% of the numerical results. For high crack densities, however, Eq. (11) shows significant differences from the numerical results; this is highlighted in the inset to Fig. 3. Note that the log-scale implies large differences. A comparison of numerical and theoretical results reveals that Eq. (11) is valid for $\left(\frac{h_f \overline{E}_f}{L\overline{E}_s}\right) <\sim 25$.

The high crack density regime is more clearly illustrated by plotting the effective modulus normalized by the effective modulus of just the substrate, as shown in Fig. 4. The analytical form given as Eq. (14) reveals that the effective modulus should only be a strong function of the crack spacing relative to substrate thickness, and this is indeed the case. It is worth noting that for each case shown in Fig. 4, the crack spacing

Table 1
Examples of multi-layer properties for parameter studies

Case	Film properties			Substrate properties			Multi-layer properties		
	h_f	E_f	v_f	h_s	E_s	v_s	$1-\alpha$	β	$\frac{\overline{E}_f h_f}{\overline{E}_s h_s}$
1	12.5 nm	110 GPa	0.35	63.5 μm	1.5 MPa	0.49	3.2×10^{-5}	0.020	12.5
2	250 nm	110 GPa	0.35	63.5 μm	1.5 MPa	0.49	3.2×10^{-5}	0.020	250
3	50 nm	91 GPa	0.39	63.5 μm	1.5 MPa	0.49	3.8×10^{-5}	0.020	42.8
4	3 μm	4 GPa	0.40	63.5 μm	1.5 MPa	0.49	8.3×10^{-4}	0.020	114
5	1 μm	4 GPa	0.40	63.5 μm	1.5 MPa	0.49	8.3×10^{-4}	0.020	38
6	1 μm	330 MPa	0.40	63.5 μm	1.5 MPa	0.49	0.01	0.019	3.1

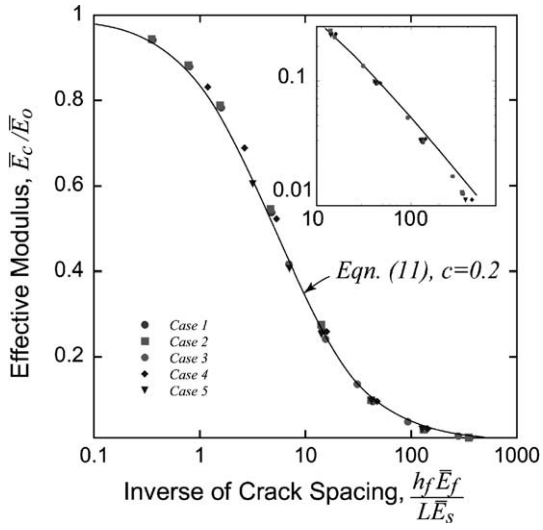

Fig. 3. Effective modulus of the cracked film/substrate as function of crack spacing.

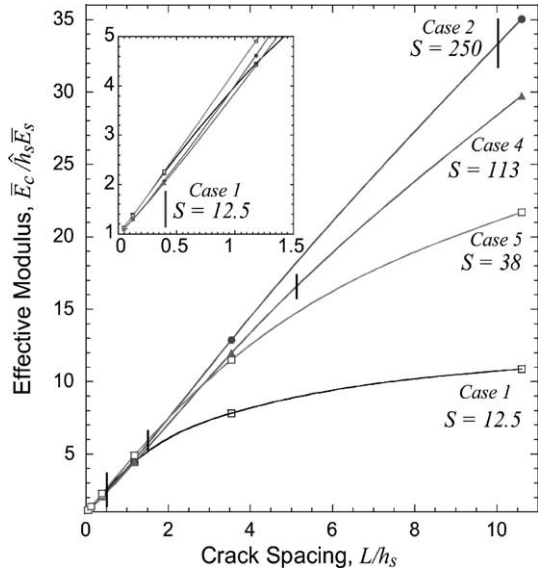

Fig. 4. Effective modulus of the multi-layer relative to that of just the substrate for high crack densities, as function of crack spacing.

exceeds the film thickness by more than three orders of magnitude. Also, it is important that despite relatively large crack densities, the effective modulus of the multi-layer is still several times larger than that of just the substrate. This is supported by experiments on electrostrictive actuators that have similar crack densities and effective moduli to those shown in Fig. 4 (Begley et al., 2005). The vertical lines in Fig. 4 represent the cut-off values for each case where Eq. (11) becomes valid. To the right of the vertical lines, crack densities are low enough such that Eq. (11) can be accurately applied. Beneath the cut-off values, adjacent shear zones begin to interact and the modulus is nearly a linear function of the crack spacing. In this regime, Eq. (14) should be used.

The inset to Fig. 4 reveals that, in regimes where crack spacing is comparable to the film thickness, differences on the order of 10% can arise for different combinations of film thickness and modulus. Unfortunately, these differences are not a systematic function of the dimensionless parameters identified previously, nor is an effective material/thickness combination obvious. Considering that in this regime, the shear transfer zones span the entire crack spacing, and the spacing is comparable to the substrate thickness, this is perhaps not surprising. In this regime, the deformation does not vary predominantly in the x-direction, but in the y-direction as well. It is likely that the details of crack tip deformation play a more significant role in these regimes.

4.2. Energy release rates for channeling crack formation

The steady-state energy release rate for isolated channeling cracks is shown to be a strong function of elastic mismatch in Fig. 5. Whether or not a crack is influenced by its neighbors is a function of the dimensionless combinations identified earlier. The results in Fig. 5 reflect scenarios where increasing the crack spacing does not change the crack driving force. It is obvious that the results scale with $1/(1-\alpha)$, such that enormous increases in crack driving force are possible for highly compliant substrates. A least-squares fit to the data yields $c \approx 0.22$ in Eq. (15b). Two data points are included at $\alpha = 0.99$; that from the present study, and that from Beuth's paper (1992). These points illustrate an important point: the energy release rate is only independent of the stress in the substrate for sufficiently thin films, such that the film carries a negligible contribution to the total load applied to the multi-layer. Our data point at $\alpha = 0.99$ corresponds to a 1 μm polymer film with relatively low modulus (330 MPa) on top of a 63 μm thick elastomer (the last case in Table 1). By comparison with Beuth's result, it is clear that this thickness ratio cannot be regarded as small—i.e. the substrate is not semi-infinite in our case. This is illustrated by the fact that $\overline{E}_f h_f / \overline{E}_s h_s \approx 3$. Beuth determined the thickness of the substrate such that it did not affect his result. He does not explicitly state layer dimensions, hence the question mark in the labeling of Fig. 5. Thus, the discrepancy is probably a result of different dimensions in the model. A more recent study by Huang et al. (2003) also reports values that are slightly larger than Beuth's results.

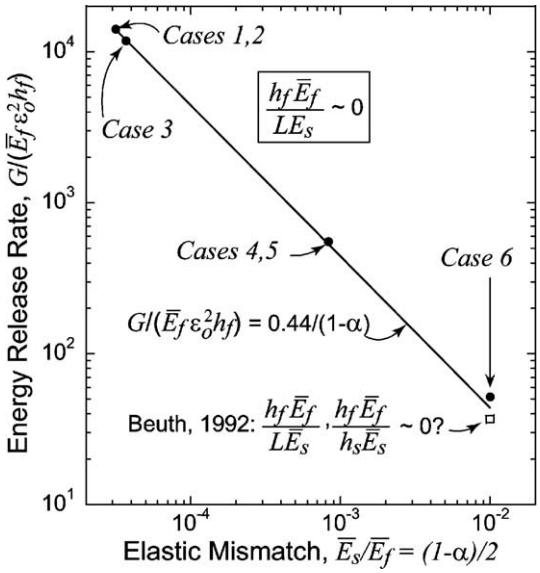

Fig. 5. Energy release rate for isolated cracks as a function of large material mismatch.

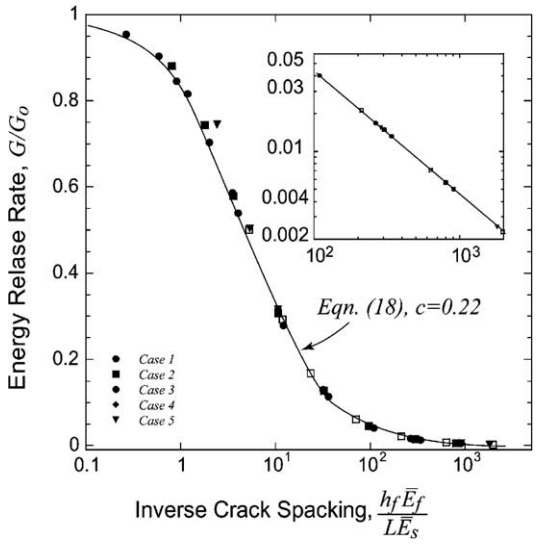

Fig. 6. Energy release rate for channeling crack formation as function of crack spacing.

To provide a physical context for the magnitudes of energy release rate shown in Fig. 5, consider a 100 nm thick film amorphous silica film on top of a semi-infinite substrate strained to 0.2%. The energy release rate for an isolated crack in an amorphous silica film on an aluminum substrate is $G \approx 0.063$ J/m^2 ($G/\overline{E}_f \varepsilon^2 h_f = 1.976$, e.g. Beuth, 1992). The energy release rate for the film on top of a glass polymer is $G \approx 1.28$ J/m^2 ($G/\overline{E}_f \varepsilon^2 h_f \approx 40$). The same film on a poly(dimethyl siloxane) (PDMS)-based elastomer is $G \approx 320$ J/m^2 ($G/\overline{E}_f \varepsilon^2 h_f = 10,000$). Thus, sub-micron films are not likely to crack due to thermal expansion mismatch when deposited on substrates with similar elastic properties (unless they have exceedingly low toughness values), and upon mechanical loading the substrates are susceptible to failure before film cracking. Hence, compliant substrates may prove useful in film toughness measurements on films with thickness less than ~1 μm.

Fig. 6 shows the energy release rate for several different material combinations as a function of normalized crack spacing. The energy release rate has been normalized by the isolated crack result, i.e. the results from Fig. 5. The theoretical form given as Eq. (19) is also shown in Fig. 6; taking $c = 0.22$ produces the solid line shown in the figure. Thus, a single fitting constant yields the correct dependence on crack spacing (Eq. (19a)) and elastic mismatch (Eq. (19b)). The inset to Fig. 6 shows the behavior for large crack densities. Using $c = 0.22$ yields results that are less accurate for small crack densities (with increasing error for decreasing elastic mismatch), but highly accurate for very large crack densities.

5. Discussion of the electro-mechanical performance of actuators with cracked electrodes

In an ideal system, electrostrictive actuators are fabricated using highly compliant electrodes separated by a highly compliant substrate, thus maximizing the actuation strain. There are materials and techniques available that can be used to produce more compliant electrodes than metal films, such as conductive carbon grease. However, these pose significant fabrication and reliability challenges (Pelrine et al., 1998). Here, we consider the possibility of introducing cracks in a blanket conductive layer to reduce the effective in-plane modulus, and thus increase the actuation strain. The previous results can be used to evaluate the performance of these actuators.

We consider the following scenario: a cracked multi-layer initially has equally distributed charge across all cracked islands (see Fig. 1), which creates an electric field transverse to the multi-layer, E_a. When the charge is equally distributed, the electric field across the cracks is zero. A voltage increment, ΔV_a, is then applied to the island(s) with an electrical lead attached; prior to breakdown across neighboring cracks, an electric field is generated across the cracks equal to $\Delta V_a/2\delta$.

Two questions are of immediate interest: (1) What is the minimum voltage increment that must be applied to the configuration shown in Fig. 1, such that breakdown across the cracks and charge is distributed across the islands? (2) What is the maximum voltage increment that can be applied to the multi-layer, before the resulting actuation strain prevents breakdown between the crack surfaces? Since the modulus of the cracked layer is known as a function of crack spacing, one can determine the required crack spacing for operation.

Breakdown occurs across the cracks when $\Delta V_a/2\delta > E_b$, where E_b is the breakdown electric field in air. Noting that the increment in electric field applied to the actuator is given by $\Delta E_a = \Delta V_a/2h_s$, the breakdown condition for the cracks can be written in terms of the increment in electric field applied to the actuator:

$$\frac{\Delta E_a}{E_b} \geqslant \frac{\delta}{h_s}. \tag{21}$$

The total axial strain in the multi-layer is the superposition of those due to an external applied load, σ_a, and the applied electric field:

$$\varepsilon = \frac{\kappa_0 \kappa (E_a + \Delta E_a)^2}{4\overline{E}_s} + \frac{\sigma_a}{\overline{E}_c}, \tag{22}$$

where $\kappa_0 = 8.854 \times 10^{-12}$ F/m is the permittivity of free space, κ is the electric constant of the dielectric and σ_a is the average applied stress. Using Eq. (17), one obtains the following condition needed to transmit charge across the cracked layers:

$$\frac{\Delta E_a}{E_b} \geqslant 0.2\left(\frac{h_f \overline{E}_f}{h_s \overline{E}_0}\right)\left(\frac{\sigma_a}{\overline{E}_s} + \frac{\kappa_0 \kappa (E_a + \Delta E_a)^2}{4\overline{E}_s}\frac{\overline{E}_c}{\overline{E}_s}\right). \tag{23}$$

There are two limits to this equation: the first represents the minimum applied electric field required to maintain conductivity, while the second corresponds to the maximum applied electric field where conductivity is lost.

In exploring solutions to Eq. (23), it is convenient to introduce the parameters $\varepsilon_m = \sigma_a/\overline{E}_c$ and $\varepsilon_b \equiv \kappa_0 \kappa E_b^2/2\overline{E}_s$; these represent the applied mechanical strain, and the electrostatically induced strain when the applied field equals the breakdown field of the cracks, respectively. The applied electric field (and increment) are normalized by the breakdown field, such that: $\Delta\widehat{E}_a \equiv \Delta E_a/E_b$ and $\widehat{E}_a \equiv E_a/E_b$. In terms of these parameters, Eq. (23) yield the following solutions:

$$\Delta\widehat{E}_a = \frac{\left(1 - 0.4\left(\frac{h_s\overline{E}_f}{h_f\overline{E}_0}\right)\left(\frac{\overline{E}_c}{\overline{E}_s}\right)\widehat{E}_a\varepsilon_b\right) \pm \sqrt{1 - 0.8\varepsilon_b\left(\frac{h_s\overline{E}_f}{h_f\overline{E}_0}\right)\left(\frac{\overline{E}_c}{\overline{E}_s}\right)\left(\widehat{E}_a + 0.2\left(\frac{h_s\overline{E}_f}{h_f\overline{E}_0}\right)\varepsilon_m\right)}}{0.4\left(\frac{h_s\overline{E}_f}{h_f\overline{E}_0}\right)\left(\frac{\overline{E}_c}{\overline{E}_s}\right)\varepsilon_b}. \tag{24}$$

When the breakdown field across the cracks is $E_b < 7.5$ MV/m (a typical value for air is ~3 MV/m for crack openings large enough to ignore Paschen's effect, wherein the breakdown voltage is gap-dependent), $\varepsilon_b < 0.001$. Expansion of Eq. (24) for small values of ε_b simplifies the results considerably. In this case, the minimum increment in applied electric field that will lead to breakdown across the cracks is

$$\Delta\widehat{E}_{a,\min} = 0.2\left(\frac{h_f\overline{E}_f}{h_s\overline{E}_0}\right)\left[\frac{\sigma_a}{\overline{E}_s} + \frac{\overline{E}_c}{\overline{E}_s}\left(\frac{\kappa_0\kappa(E_a)^2}{4\overline{E}_s}\right)\right]. \tag{25}$$

The same result is obtained directly from Eq. (23) if one assumes $\Delta E_a \ll E_a$. The minimum required increment in the applied electric field increases with applied voltage and applied stress, since both act to open the cracks. Note that in terms of the average stress applied to the layer, the crack spacing does not play a role; however, in terms of a mechanical strain applied to the multi-layer, the crack spacing plays role since $\sigma_a = \overline{E}_c \varepsilon_m$. In either case, the minimum applied electric field increment that will distribute charge increases with increasing crack spacing.

The maximum increment that can be applied before the actuator strain is large enough to prevent breakdown across the cracks is

$$\Delta \widehat{E}_{a,\max} = 10 \frac{\overline{E}_s}{\overline{E}_c} \left(\frac{h_s \overline{E}_0}{h_f \overline{E}_f} \right) \left(\frac{\overline{E}_s}{\kappa_0 \kappa (E_b)^2} \right) - 2\widehat{E}_a. \tag{26}$$

For realistic breakdown fields across the cracks, breakdown *through the dielectric* occurs for parameters that imply the second term is negligible compared to the first term. Thus, as the necessary breakdown field across the cracks increases, the maximum allowable applied electric field decreases. Similarly, as the effective modulus of the cracked multi-layer increases (e.g. via increasing crack spacing), the maximum allowable voltage decreases because crack openings get larger. Put another way, as the required breakdown field over the cracks becomes larger or the modulus of the crack layers increases, electrical performance is governed by a loss of charge distribution in the electrodes.

It should be emphasized that these results, together with Eqs. (13) and (14) can be used to determine the maximum allowable crack spacing that will maintain functionality. Eq. (26) is a function of crack spacing, when one considers that $\sigma_a = \overline{E}_c \varepsilon_m \approx \overline{E}_c \varepsilon$. Thus, for a given applied strain, increases in crack spacing (which lead to increases in modulus) lead to an increase in the minimum operating voltage and a decrease in the maximum operating voltage. The ideal situation is a heavily cracked film, which leads to smaller crack openings. Generally speaking, neither limit is particularly worrisome (particularly the upper limit). The operating electric fields for electrostatic actuators are generally much larger than breakdown field for a cracked film; the crack openings are so small that breakdown easily occurs over the cracks.

To illustrate this, consider the gold/silicone multi-layers described by Begley et al. (2005). The dimensions of the multi-layer are given as *Case 1* in Table 1. A multi-layer such as that shown in Fig. 1 is clamped around the outer edges and loaded with a large spherical indenter (with radius comparable to the span) in the direction transverse to the multi-layer. The electrically induced in-plane strain enables one to control the transverse stiffness of the membrane. The dimensions and properties are such that the first term in parenthesis on the right hand side of Eq. (25) is approximately unity. Maximum strains (including both indentation strains and electrically-induced strains) were on the order of 10%. Mechanical measurements revealed $\overline{E}_c \sim (1-5)\overline{E}_s$ (for crack spacing in the range $L \sim (0.1-1)h_s$).

Using the results presented in this section, the theoretical minimum increment in applied actuator field necessary to distribute charge across the cracks under maximum indentation load is $\Delta E_a \sim 0.3 E_b \approx 3 \times 10^5$ V/m. This implies that breakdown between the crack faces occurs (for a 128 μm thick dielectric) at applied voltage increments of ~40 V—assuming a breakdown field in air of $E_b = 1$ MV/m. Paschen's effect implies that the breakdown across the cracks may increase for micron-scale crack openings. However, this effect (or the presence of a different material inside the cracks that has a higher dielectric constant) would increase the breakdown voltage by less than an order of magnitude for micron-scale crack openings. Much larger operating voltages (~1 kV) are required to generate meaningful actuation strains, and hence, charge distributes in the cracked film throughout the entire indentation experiment. The required operating voltages are much larger than the breakdown voltage across the cracks, because the crack openings are much smaller than the dielectric thickness.

6. Concluding remarks

The present analysis should prove useful in estimating the mechanical performance of thin stiff layers on highly compliant substrates, both in terms of stress–strain response and the likelihood of crack formation. A key result is that the steady-state energy release rate for channeling cracks scales with $1/(1-\alpha)$, such that seemingly insignificant differences in elastic mismatch can have an enormous influence crack formation. Two key implications of the present analyses are that heavily cracked multi-layers still can exhibit stiffness much larger than the substrate, and that dielectric breakdown over the cracks is likely. With regards to electro-mechanical actuators, increasing the crack density improves performance by increasing the likelihood of charge distribution for a given applied electric field.

It should be emphasized that the preceding discussions are based upon the assumption that thickness of the stiff, conductive layer is far smaller than the dielectric thickness. The key element of the linear analysis presented here is that the crack openings scale with the electrode thickness; this implies that the breakdown field for the cracks is much smaller than the applied electric fields required for significant actuation strains. Naturally, adopting a non-linear material description for elastomers and considering large strains will narrow the range of acceptable applied fields. However, when the conductive films are sufficiently thin, and moderately cracked, the minimum and maximum applied electric fields are orders of magnitude different from typical operating values. It is unlikely that the increase in crack opening displacements due to non-linear behavior larger strains will prevent operation at small strains.

Acknowledgments

MRB and HBS are grateful for the contributions Mr. Orion N. Scott (UVA), and Mr. Michael H. Jones (UVA), for their work on the electrostrictive experiments discussed in Section 5, and Prof. M.L. Reed (UVA) for an insightful discussion regarding charge distribution in cracked electrodes. MRB gratefully acknowledges the support of the National Science Foundation through Award #9984517. HBS gratefully acknowledges the support of the National Science Foundation through Award #0348448 and the David and Lucile Packard Foundation.

References

Begley, M.R., Begley, C.J., 2003. Interfacial debonding around rectangular features in multi-layer structures. Interface Science 11, 319–327 (Special Issue on the Mechanics of Interfaces).

Begley, M.R., Scott, O.N., Bart-Smith, H. Jones, M.H., Reed, M.L., 2005. Electro-mechanical response of elastomer membranes coated with ultra-thin metal electrodes. Journal of the Mechanics and Physics of Solids, in press.

Beuth, J.L., 1992. Cracking of thin bonded films in residual tension. International Journal of Solids and Structures 29, 1657–1675.

Beuth, J.L., Klingbeil, N.W., 1996. Cracking of thin films bonded to elastic–plastic substrates. Journal of the Mechanics and Physics of Solids 44, 1411–1428.

Cook, T.S., Erdogan, F., 1972. Stresses in bonded materials with a crack perpendicular to the interface. International Journal of Engineering Science 10, 677–697.

Delannay, F., Warren, P., 1991. On crack interaction and crack density in strain-induced cracking of brittle films on ductile substrates. Acta Metallurgica et Materialia 39, 1061–1072.

Huang, R., Prevost, J.H., Huang, Z.Y., Suo, Z., 2003. Channel-cracking of thin films with the extended finite element method. Engineering Fracture Mechanics 70, 2513–2526.

Hutchinson, J.W., Jensen, H.M., 1990. Models of fiber debonding and pullout in brittle composites with friction. Mechanics of Materials 9, 139–163.

Hutchinson, J.W., Suo, Z., 1992. Mixed mode cracking in layered materials. In: Hutchinson, J.W., Wu, T.Y. (Eds.), Advances in Applied Mechanics, vol. 29. Academic Press, San Diego, pp. 63–191.

McCartney, L.N., Schoeppner, G.A., Becker, W., 2000. Comparison of models of transverse ply cracks in composite laminates. Composite Science and Technology 60, 2347–2359.

Nahta, Z., Moran, B., 1995. Crack spacing in brittle films on dissimilar planar and axisymmetric elastic substrates. Engineering Fracture Mechanics 52, 513–524.

Pelrine, R.E., Kornbluh, R.D., Joseph, J.P., 1998. Electrostriction of polymer dielectrics with compliant electrodes as a means of actuation. Sensors and Actuators A 64, 77–85.

Pelrine, R., Kornblush, R., Joseph, J., Heydt, R., Pei, Q., Chiba, S., 2000. High-field deformation of elastomeric dielectrics for actuators. Materials Science and Engineering C 11, 89–100.

Thouless, M.D., 1990. Crack spacing in brittle films on ductile substrates. Journal of the American Ceramic Society 73, 2144–2146.

Zak, A.R., Williams, M.L., 1963. Crack point stress singularities at a bi-material interface. Journal of Applied Mechanics 30, 142–143.